Published in the Proceedings of the 16th International Aluminum Alloys Conference (ICAA16) 2018
ISBN: 978-1-926872-41-4
by the Canadian Institute of Mining, Metallurgy & Petroleum

THE ELEMENTAL DISTRIBUTION AND PRECIPITATION KINETICS OF CHROMIUM DISPERSOIDS IN Al-Mg-Si ALLOYS

*M. Kenyon[1], J. Robson[1], J. Fellowes[2] and Z. Liang[3]

[1]School of Materials Science
University of Manchester, Manchester, UK
*(*Corresponding author: michael.kenyon@postgrad.manchester.ac.uk)*

[2]School of Earth and Environmental Sciences
University of Manchester, Manchester, UK

[3]Novelis R&T centre
Sierre, Switzerland

ABSTRACT

Dispersoids play a significant role in the recrystallization and texture development for wrought Al-Mg-Si (6xxx series) alloys by inhibiting grain boundary motion. It is therefore important to understand the precipitation kinetics of such particles. It is the additions of Mn and Cr in Al-Mg-Si based systems that can lead to dispersoid phases being formed. These phases are currently thought to nucleate on β'-Mg_2Si via an intermediate semi-coherent precipitate. Scanning transmission electron microscopy (STEM) has been conducted to study the precipitation of α-Al(CrFe)Si and α'-AlCrSi dispersoids. Corresponding electron dispersive spectroscopy (EDS) has been used to distinguish the dispersoids. The volume fraction and size distribution of dispersoids has been measured as a function of distance across a grain. Electron probe microanalysis (EPMA) has been conducted to study the inhomogeneity of elements in the cast structure and the effect on dispersoid precipitation. Dispersoid free regions have been observed in the microstructure correlating to regions depleted in the dispersoid forming elements.

KEYWORDS

Dispersoids, Electron probe micro analysis, Transmission electron microscopy

INTRODUCTION

Al-Mg-Si (6xxx series) based alloys are increasingly being used in the automotive industry. The primary reason is to reduce the weight of vehicles, resulting in a reduction of CO_2 emissions and increased fuel efficiency. The demand for 6xxx series is predicted to increase over the coming decade. Due to the high cost and CO_2 emissions produced by raw extraction of aluminium, close loop recycling of these alloys becomes a more important process. However recycling of automotive alloys can be difficult due to pick up of impurity elements such as Mn, Cr and Fe. The addition of these elements can form dispersoid particles during early heat treatment processes. Although a controlled population of dispersoids is necessary to control the grain structure during thermo-mechanical processing, a significant change to the dispersoid population due to a composition change could profoundly influence the final microstructure, affecting the final properties of the material. More research is required on the precipitation and effect of additional minor alloying elements; in order to increase the 6xxx series alloys recyclability.

Three different types of dispersoids have been identified in 6xxx alloys when Cr and Mn are present. These include the α-Al(CrMnFe)Si, α'-AlCrSi and θ-AlCr phases (Robinson, 1994; Buchanan, Ribis, Garnier & Colas, 2016; Lodgaard & Ryum, 2000; Strobel, Sweet, Easton & Nie, 2010). Robinson (1994) reported that the α'- $Al_{13}Cr_4Si_4$ has a face centered cubic (FCC) structure, while the θ - Al_7Cr has a monoclinic structure (Buchanan et al., 2016). Lodgaard and Ryum (2000b) found that when a high ratio of (Mn,Cr):Fe is present, the α-$Al_{15}(MnCrFe)_3Si_2$ phase is observed to adopt a simple cubic (SC) structure. It has also been found that a phase change occurs from $Al_{15}(MnFe)_3Si_2$ SC to $Al_{12}(MnFe)_3Si$ body centered cubic (BCC) with increased homogenisation time and temperatures as further Fe diffuses to the dispersoids (Strobel et al., 2010; Yoo, Shan, Moon & Maeng, 1999). When Mn or Cr is absent, the dispersoid phase remains α, of a composition that omits the missing element.

Lodgaard and Ryum (2000b) studied the precipitation of dispersoids containing Mn, Cr and Mn+Cr. They found that Mn and Mn+Cr dispersoids precipitate on a semi coherent phase termed the 'u-phase', from around 400°C. A number of dispersoids precipitate from each u-phase particle, resulting in a string of dispersoids. The u-phase precipitates at approximately 350°C on β`-$Mg_2Si$ particles until they are completely dissolved. In a separate study, the precipitation of Cr dispersoids was investigated but the precipitation sequence was not determined (Lodgaard & Ryum, 2000a). More recent studies have also shown the requirement of the β`-Mg_2Si as a nucleation site for Mn dispersoids. A number of studies (Farah, Djemmal, Guemini & Serradj, 2012; Hu, Ogura, Tezuka, Sato & Liu, 2010) reported that Mn dispersoids had precipitated in a string along the <100> Al direction. As this coincided with the traces of the β`-$Mg_2Si$ phase, Farah et al (2011) suggested the Si contained in the β` phase could act as a preferential nucleation site for the dispersoids. Hu et al. showed TEM evidence of Mn dispersoids precipitating directly on the β`-Mg_2Si phase. In both studies, there was no indication of any other intermediate phase such as the u-phase that the dispersoids had precipitated on.

Microprobe measurements to determine the elemental segregation in 6xxx series cast microstructures have been conducted (Lodgaard & Ryum, 2000a, 2000c; Hu et al., 2010). Mg and Si were found to segregate between the secondary dendrite arms and towards grain boundaries. Cr was relatively uniformly distributed but indicated segregation towards the dendrite centres. As the solid solubility of Fe in aluminium is low (<0.05wt%), its concentration was below the resolution of the microprobe measurements for these studies (Lodgaard & Ryum, 2000a, 2000b). However the segregation profile of Fe has been demonstrated through Scheil calculations (Samaras & Haidemenopoulos, 2007). Samaras and Haidemenopoulos (2007) predicted that Fe segregates between the secondary dendrite arms. In addition, due to the slow diffusion of Fe in FCC aluminium, the profile is not expected to change significantly during homogenisation.

A number of studies have considered the final distribution of dispersoids (Lodgaard & Ryum, 2000b, 2000c; Remøe, Marthinsen, Westermann, Pedersen, Røyset & Reiso, 2016). Lodgaard and Ryum (2000c) found that the uniformity of Mn, Cr and Mn+Cr dispersoids was dependent on heating rate. With quicker heating rates, the dispersoids become less uniform with a higher density towards the edges of the

dendrite arms. They revealed that the preferential nucleation sites for the dispersoids are the regions where β`-Mg_2Si particles form with the highest density. This occurs were the segregation of Mg and Si is highest, between the dendrite arms and closer to the grain boundaries. This was in agreement with other recent studies on Mn dispersoids (Remøe, Marthinsen, Westermann, Pedersen, Røyset & Reiso, 2016).

In this study, two Al-Mg-Si alloys with high levels of Cr (>0.4wt%) were used in order to study the as cast elemental distribution and the effect of grain refiner. In addition, an evaluation of the precipitation kinetics of Cr containing dispersoids was also conducted in both alloys.

EXPERIMENTAL

The 6xxx series ingots received were DC-cast by Novelis R&T centre, Sierre, Switzerland and measured approximately 220 x 195 x 40 mm. Two alloy compositions were investigated in this paper and are given in table 1. Alloy A had 0.12wt% of TiB_2 of grain refiner added while alloy B had no grain refiner.

Table 1. 6xxx series alloy compositions investigated (wt%), aluminium balanced

Alloy	Mg	Si	Fe	Cr	Ti	TiB_2
A	0.63	0.65	0.21	0.41	0.01	0.12
B	0.64	0.65	0.22	0.46	<0.01	0

The segregation of elements in the cast structure was studied via Electron Probe Micro Analysis (EPMA). Measurements were conducted on a JEOL JXA-8530F EPMA equipped with 4 Wave Dispersive Spectrometers (WDS) containing TAP, LiF(L), PET(L) and LDE crystals. A step size of 2μm was used for the quantitative line scans. Two line scans per sample from two different locations in the ingot were conducted. Qualitative maps were taken at 15kV, 43 nA beam current. The dwell time was 30ms per point with a field of view of 512μm. It should be noted that the size of the x-ray interaction volume is likely over an order of magnitude smaller than the interdendritic spacing. The as-cast samples for EPMA were ground down to 2500SiC. Polishing was conducted at 3μm grit with a final OP-S polish performed for 30 seconds. For TEM analysis, 10x10x10mm as-cast samples were heated at a rate of 50°C/hour from room temperature to 450°C and 550°C. At 450°C the samples were quickly water quenched. After heating to 550°C, the sample was held for 10 hours before the water quench in order to represent a typical industrial homogenisation regime. An air circulating furnace with temperature control within ±5°C was used. The samples were ground to a 100μm thickness with the final thinning achieved using a Struers Tenupol electropolisher. The electrolyte was a solution of 90:10 Methanol:Perchloric acid conducted at -35°C, 21V. STEM imaging was performed on a FEI Talos F200A microscope equipped with Super-X EDXS detectors. To study the dispersoid distribution, an additional sample was heated at 50°C/hour to 550°C and held for 20 hours before a water quench. This sample was prepared similar to the cast EPMA samples and etched using a 20% sulphuric acid solution at 70°C for 2 minutes in order to highlight the dispersoid distribution using a Keyence optical microscope.

RESULTS AND DISCUSSION

Elemental distribution

Figures 1 and 2 show qualitative elemental maps and quantitative line scans of the cast structures for alloy A and B respectively. As can be seen from the secondary electron micrographs and corresponding elemental maps in Figures 1(a) and 2(a), alloy A has an equiaxed grain structure whereas alloy B has a larger more columnar structure. This is to be expected as alloy A has the addition of TiB_2 grain refiner. The grain refiner has not changed the sense of segregation (i.e. the elements segregate in the same direction in both alloys A and B with respect to the dendrite centres) but the scale over which segregation occurs is clearly different due to the refinement of alloy A.

As can be seen from the both the maps and line scans, the Mg and Si segregates away from the centre of the dendrite arms for both alloys. There is a much lower level of Si in solid solution as a large

proportion of Si is contained in the larger grain boundary eutectic particles in both alloys (indicated by 'GB particle' in Figures 1(b), 1(c) and 2(c)). The Mg and Si distribution is in agreement with other similar microprobe studies on Al-Mg-Si alloys (Lodgaard & Ryum, 2000a, 2000b, 2000c; Hu et al., 2010). Thermodynamic simulations were also conducted on JMatPro predicting the weight% element in Al against fraction solid using the Scheil-Gulliver assumption. In this assumption, no back-diffusion is allowed in the solid, and the prediction of the reactions towards the end of solidification must be treated with caution. Nevertheless, the predicted segregation direction with respect to the fraction solid is consistent with the measured segregation direction with respect to the position within a dendrite (assuming the fraction solid correlates directly with position in the dendrite from center to edge). For example, the simulations shown in Figure 3(a) indicate a similar segregation for Mg and Si with the current study. Fe has a very low solubility limit in Al (<0.05wt%), however there is indication of segregation away from the dendrite centres. This can be seen in Figures 1(a) and 2(a) for both alloy A and B respectively. In addition, the line scans for both alloys show a small increase in Fe in the vicinity of the grain boundary particles (or towards the dendrite centre in Figure 2(a)). The majority of Fe is located in the eutectic particles located on the grain boundaries, as shown in the qualitative maps for alloys A and B. The segregation profile agrees with the thermodynamic simulation in Figure 3(b) in addition to other simulated results in literature (Samaras & Haidemenopoulos, 2007). The spikes in concentration of some elements towards the end of solidification correspond to invariant reactions forming the primary intermetallic particles.

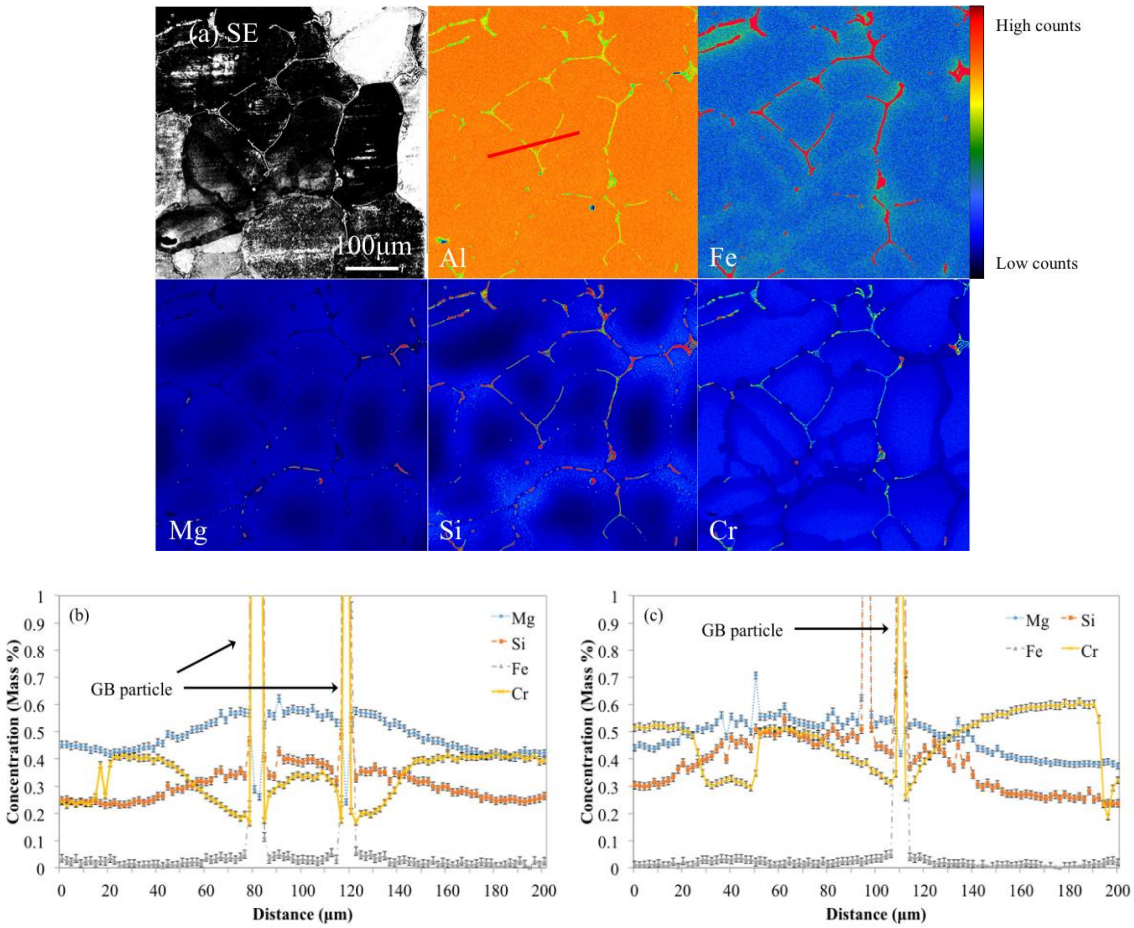

Figure 1. (a) EPMA qualitative map showing the distribution of elements in the as cast structure, (b) quantitative line scan indicated by the red line, and (c) additional quantitative line scan located in a different region on the sample

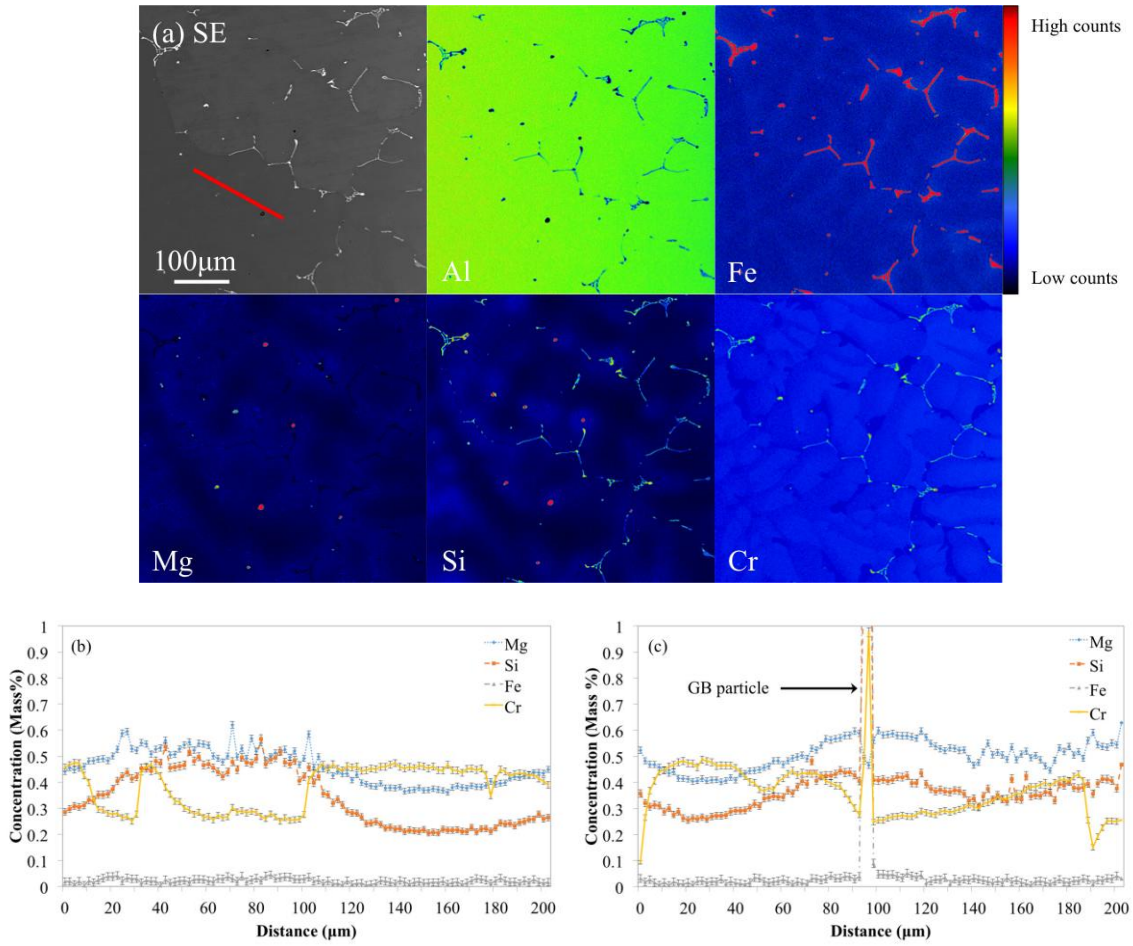

Figure 2. (a) EPMA qualitative map showing the distribution of elements in the as cast structure, (b) quantitative line scan indicated by the red line, and (c) additional quantitative line scan located in a different region on the sample

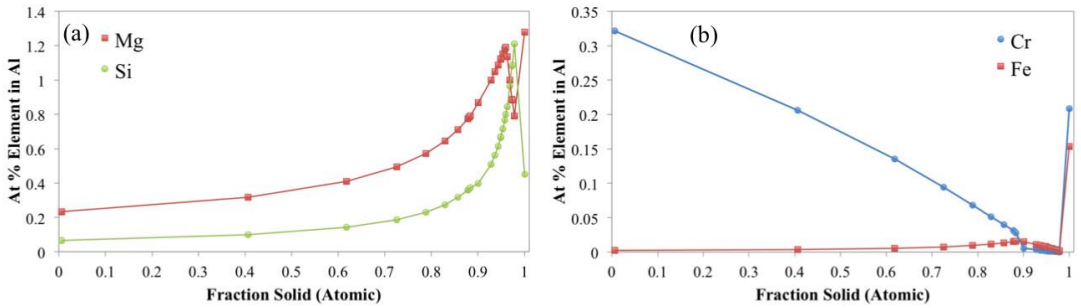

Figure 3. Thermodynamic simulations conducted on JMatPro displaying the atomic weight % element in Al against fraction solid for (a) Mg, Si and (b) Cr, Fe in alloy A

Cr is found to segregate towards the dendrite centre in both alloys, which is predicted in the thermodynamic simulation displayed in Figure 3(b). However, within the dendrite centres, the Cr is relatively uniformly distributed in both alloy A and B, in agreement with other studies (Lodgaard & Ryum, 2000a, 2000c). The quantitative line scans in Figures 1(b), 1(c) and 2(c) show a gradual depletion of Cr

adjacent to the grain boundary particles (indicated by 'GB particle' in Figures 1(b), (c) and 2(c)). This is as expected as some Cr diffuses during solidification to form the coarse grain boundary constituent phase α-AlFeCrSi. However, as can be seen from the qualitative maps in Figures 1(a) and 2(a), both alloys show other regions of significantly lower Cr in the vicinity of grain boundaries where no eutectic is present, and between grain boundary eutectic particles. These regions are presented more clearly in Figure 4, which displays a magnified Cr map for alloy A. These large (up to 30 μm diameter) pockets that are strongly depleted in Cr correspond to the final Cr depleted liquid to solidify. It can be seen that these regions occur between regions of grain boundary where the eutectic intermetallic is formed. It should be noted that the partitioning behavior of Cr during solidification may be strongly affected by alloying additions and the invariant reaction in the binary Al-Cr system is only marginally peritectic, and so the segregation behavior can be significantly influenced by minor additions (Kurtuldu, Jessner & Rappaz, 2015). The focus of this study was understanding how the segregated cast structure influences the final dispersoids distribution, so the origins of the low Cr pockets were not explored in further detail.

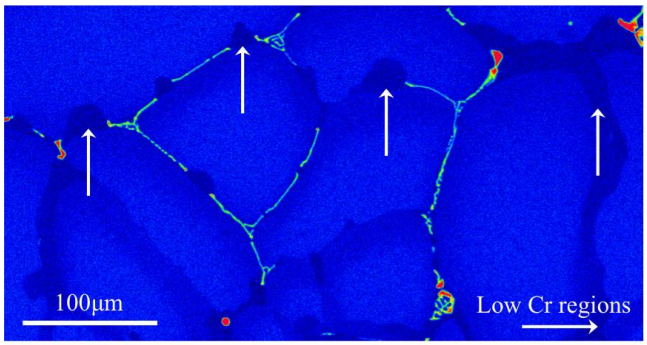

Figure 4. A magnified EPMA qualitative map for Cr in alloy A, indicating the regions with significantly lower Cr

In order to show how the low Cr regions affect the dispersoid distribution, an additional alloy A sample was heated to 550°C and held for 20 hours. Figure 5(a) shows an optical micrograph of the general dispersoid distribution in this sample. Indicated in Figure 5(a) are clear regions were no dispersoids have formed. Figure 5(b) shows a STEM micrograph of an example region that is completely free of dispersoids adjacent to a grain boundary. These regions coincide with the low Cr regions between the grain boundary eutectic. The dispersoid free regions will affect further thermo mechanical processing of the alloy due to the dispersoids playing a significant role in recrystallisation.

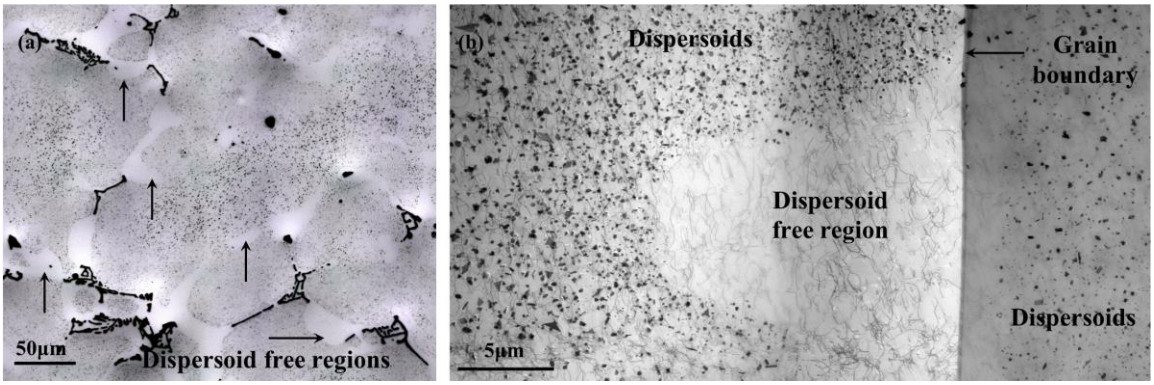

Figure 5. (a) An optical micrograph showing the dispersoid distribution after heating to 550°C and holding for 20 hours in alloy A. (b) A STEM bright field micrograph showing a region with no dispersoids adjacent to a grain boundary under the same heat treatment conditions

Precipitation of Dispersoids

Figure 6 shows bright field STEM micrographs of the general morphologies of dispersoids after continuous heating to 550°C and holding for 10 hours in alloy A. As can be seen from Figure 6(a) and (b), there are varied morphologies including spherical, rectangular, hexagonal and rod like dispersoids. Similar morphologies were also found in alloy B. Figure 6(a) shows the dispersoids 0–5 μm away from the grain boundary with a eutectic particle several microns in length on the left of the image. Figure 6(b) is 30–35 μm away from the same grain boundary.

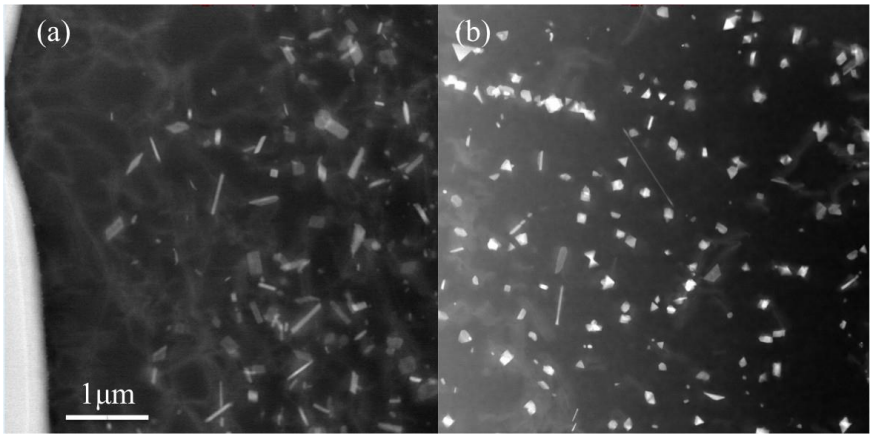

Figure 6. STEM HAADF micrographs of dispersoids after a 10 h homogenisation at 550°C in alloy A. Micrograph (a) is 0–5 μm and (b) 30-35 μm away from the grain boundary respectively

A number of micrographs were taken consecutively in a line from the grain boundary (located at 0 μm in Figure 7) towards the grain centre (35–40 μm in Figure 7) and analysed using ImageJ. 1540 dispersoids were studied in total over 8 micrographs. Figure 7 shows the effective diameter and area fraction as a function of distance away from the grain boundary with the corresponding example STEM micrographs that were analysed. The dispersoids studied consisted of two types, the α-Al(CrFe)Si and α'-AlCrSi dispersoids. The analysis shown in Figure 7 did not distinguish between these two types. From 0–5 μm, there is a lower area fraction of dispersoids compared to between 5–30 μm. This is due to the inclusion of the precipitate free zone which can be seen on the corresponding micrograph for 0–5 μm in Figure 7. From 5–10 μm there are a larger number of smaller dispersoids indicated by the increase in area fraction but decrease in size. From 10–40 μm the area fraction and size of dispersoids steadily decreases towards the grain centre. The overall decrease of dispersoids towards the grain centre is similar to other studies on Mn, Cr and Mn+Cr dispersoids (Lodgaard & Ryum, 2000b, 2000c).

The decrease in dispersoids towards the grain centre could be attributed to the segregation of Mg and Si in the cast alloy, as shown in Figures 1 and 2. Other studies have shown for Mn and Mn+Cr dispersoid systems, that the dispersoids precipitate at lower temperatures on Mg and Si containing particles (ref). In these systems, the segregation of Mg and Si results in an increase in density of β' particles towards the grain boundary. This results in a higher density of dispersoids towards the grain boundary during heating. This observation emphasizes the complexity of the influence of the segregation in the cast structure on dispersoids precipitation, since it is not only the distribution of the dispersoid forming elements (e.g. Mn and Cr) that is important, but also the segregation of the major alloying additions that form the pre-cursor phases (Mg + Si). Dispersoids will only form in regions where there is sufficient Cr, but once this critical concentration is exceeded, the local Mg and Si concentrations become important by controlling the potential to precipitate the pre-cursor phases. The optimum conditions to precipitate the maximum fraction of dispersoids require both sufficient Cr and sufficient Mg and Si. Since the local Cr concentration is low towards the dendrite edges, and the local Mg and Si are low towards the centers, this optimum condition corresponds to positions between these extremes.

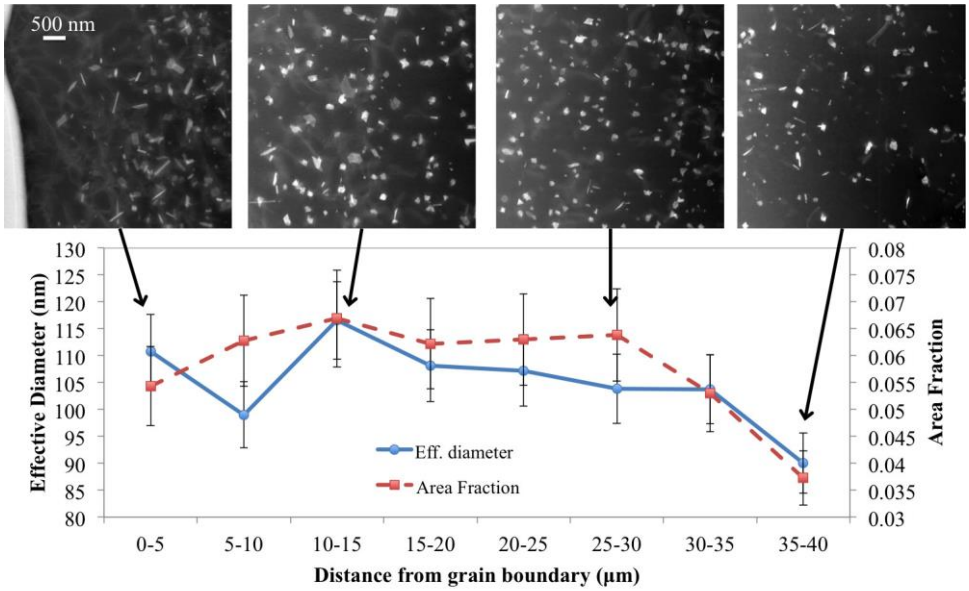

Figure 7. The average effective diameter and area fraction of dispersoids studied from the grain boundary (located at 0 µm) towards the grain centre (located at 40 µm)

Figure 8 shows dispersoids after a 10 hour homogenisation heat treatment at 550°C with corresponding EDS maps. Figure 8 shows the existence of two types of dispersoids, the α-Al(FeCr)Si and α'-AlCrSi dispersoids distinguished by the presence of Fe in the α dispersoids as indicated in the Cr and Fe maps. 13 of each type of dispersoid have been studied in alloy A. Table 2 shows the effective diameter, aspect ratio and form factor for both types of dispersoid present. Aspect ratio and form factor were chosen to represent the dispersoid morphology, as they are dependent on two different particle attributes, elongation and ruggedness respectively (Hentschel & Page, 2003). Both dispersoid types have a variation in morphology as indicated by the aspect ratio and form factor, however the α'-AlCrSi are larger than the α-Al(FeCr)Si dispersoids. Similar morphologies of dispersoids have been previously found for both α-Al(FeCr)Si and α'-AlCrSi (Buchanan et al., 2016; Lodgaard & Ryum, 2000a) under different heat treatment and processing conditions.

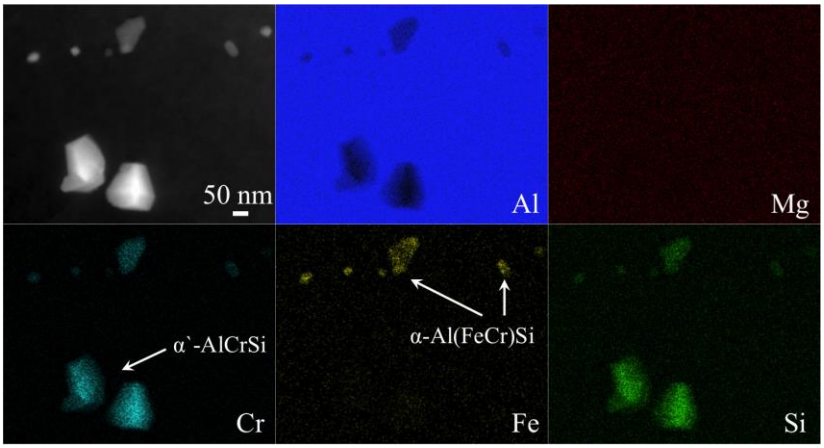

Figure 8. STEM HAADF micrograph with corresponding EDS maps after a 10 hour homogenisation heat treatment at 550°C

Table 2. The effective diameter, aspect ratio and form factor for the two types of dispersoids present after continuous heating to 550°C and holding for 10 hours

Dispersoid	Effective diameter (nm)	Aspect ratio	Form factor
α-Al(FeCr)Si	74 ± 20	1.58 ± 0.35	0.72 ± 0.09
α'-AlCrSi	162 ± 28	2.09 ± 1.49	0.60 ± 0.10

Figure 9 displays only α dispersoids distributed in alloy B after continuous heating to 450°C. The dispersoids have precipitated in a string in the <100> Al directions as indicated by the selected area diffraction pattern (SADP). Similarly to other studies for Mn and Mn+Cr dispersoids at different temperatures (Farah et al., 2011; Lodgaard & Ryum, 2000b) the dispersoids follow the alignment of the β`-Mg_2Si particles that had formed at lower temperatures. This suggests that Cr containing dispersoids follow a similar precipitation sequence to Mn and Mn+Cr dispersoids. All the dispersoids studied via EDS were of the α-Al(FeCr)Si type dispersoid and no evidence of the α'-AlCrSi dispersoid has been found in either alloy at this temperature. In both alloys A and B, the dispersoids formed in a manner as shown in Figure 9.

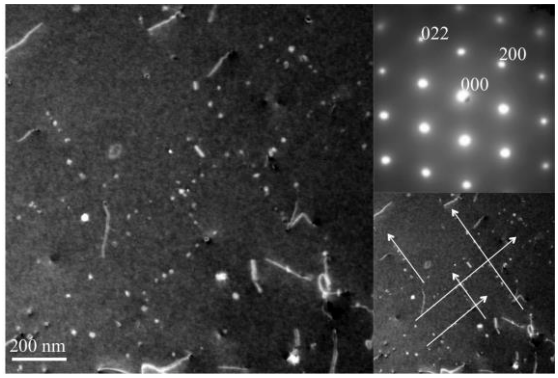

Figure 9. STEM HAADF micrograph of dispersoids distributed in lines along the <100> Al directions in alloy B after continuous heating to 450°C

CONCLUSIONS

EPMA qualitative maps and quantitative line scans have been conducted on two as cast Al-Mg-Si alloys with a high level of Cr. The dispersoid precipitation was also studied with TEM. A number of conclusions can be drawn from the current work. The addition of grain refiner in alloy A changed the grain structure and scale of elemental segregation from alloy B that contained no grain refiner. Large regions of significantly lower Cr were found in the vicinity of grain boundaries or between grain boundary eutectic in both alloys. These depleted areas resulted in dispersoid free regions after homogenisation heat treatment and could affect further thermo mechanical processing. Mg, Si and Fe segregated away from the dendrite centres in alloys A and B. The area fraction and size of dispersoids decreased from the grain boundary to the grain centre. Evidence of the α-Al(FeCr)Si dispersoids forming in a string like manner was also found in both alloys. A combination of decreasing density of dispersoids towards the grain centre, and evidence of the dispersoids forming in a string like manner, suggests the precipitation and distribution of Cr dispersoids is dependent on the segregation of Mg, Si and Cr in the cast structure. The effect of the segregation of these elements on the final dispersoids distribution is different, however. A critical local Cr level is needed to form any dispersoids and dispersoids free regions correspond to regions where this level is not reached. Where the critical Cr level is exceeded, the segregation of Mg and Si become important in controlling the nucleation of dispersoids by providing different amounts of precursor phase, thus influencing both the size and fraction of dispersoids. The observation that Cr segregates in the opposite sense to Mg and Si explains the occurrence of dispersoids free zones towards the dendrite edges (low Cr) and dispersoid depleted zones towards dendrite centers (low Mg and Si).

ACKNOWLEDGMENTS

The author gratefully acknowledges the funding support from the UK EPSRC CDT in Advanced Metallic Systems and the use of the EPSRC funded JEOL JXA-8530F FEG-EPMA, award EP/M028097/1. The author would also like to thank Novelis for their advice, funding and provision of materials.

REFERENCES

Buchanan, K., Ribis, J., Garnier, J., & Colas, K. (2016). Identification of monoclinic θ-phase dispersoids in a 6061 aluminium alloy. *Philosophical magazine letters*, 96(4), 121–131. https://doi.org/10.1080/09500839.2016.1162911

Farah, H., Djemmal, K., Guemini, R., & Serradj, F. (2011). Effect of Heat Treatment on the Formation and Distribution of Dispersoid Particles in AlMgSi. *Global Journal of Science Frontier Research Physics and Space Science.* 12(1), 45–48.

Hentschel, M., & Page, N. (2003). Selection of Descriptors for Particle Shape Characterization. *Particle & Particle Systems Characterization.* 20, 25–38.

Hu, R., Ogura, T., Tezuka, H., Sato, T., & Liu, Q. (2010). Dispersoid Formation and Recrystallization Behaviour in an Al-Mg-Si-Mn Alloy. *Journal of Materials Science and Technology.* 26(3), 237–243. https://doi.org/10.1016/S1005-0302(10)60040-0

Kurtuldu, G., Jessner, P., & Rappaz, M. (2015). Peritectic reaction on the Al-rich side of the Al-Cr system. *Journal of alloys and compounds.* 621, 283–286. https://doi.org/10.1016/j.jallcom.2014.09.174

Lodgaard, L., & Ryum, N. (2000a). Precipitation of chromium containing dispersoids in Al-Mg-Si alloys. *Materials Science and Technology*, 16, 599–604. https://doi.org/10.1179/026708300101508315

Lodgaard, L., & Ryum, N. (2000b). Precipitation of dispersoids containing Mn and/or Cr in Al-Mg-Si alloys. *Materials Science and Engineering*, A283, 144–152. https://doi.org/10.1016/S0921-5093(00)00734-6

Lodgaard, L., & Ryum, N. (2000c). Distribution of Mn- and Cr-Containing Dispersoids in al-Mg-Si Alloys. *Materials Science Forums*, 331, 945–950. https://doi.org/10.4028/www.scientific.net/MSF.331-337.945

Remøe, M., Marthinsen, K., Westermann, I., Pedersen, K., Røyset, J., & Reiso, O. (2016). The Effect of Heating Rate on the Desnity and Spatial Distribution of dispersoids during Homogenisation of 6xxx Aluminium Alloys. *Materials Science Forum*, 877, 322–327. https://doi.org/10.4028/www.scientific.net/MSF.877.322

Robinson, K. (1953). The Structure of α(AlCrSi)-$Cr_4Si_4Al_{13}$. *Acta Crystallographica*, 6(11), 854–859. https://doi.org/10.1107/S0365110X53002490

Samaras, G.N., & Haidemenopoulos. (2007). Modelling of microsegregation and homogenization of 6061 extrudable Al-alloy. *Journal of Materials Processing Technology*, 194, 63–73. https://doi.org/10.1016/j.jmatprotec.2007.03.126

Strobel, K., Sweet, E., Easton, M, Nie, J., & Couper, M. (2010). Dispersoid Phases in 6xxx Series Aluminium Alloys. *Materials Sceince Forum*, 654–656, 926–929. https://doi.org/10.4028/www.scientific.net/MSF.654-656.926

Yoo, JE., Shan, A., Moon, IG., & Maeng, SJ. (1999). A study on composition and crystal structure of dispersoids in AlMgSi alloys. *Journal of Materials Science*, 34, 2679–2683. https://doi.org/10.1023/A:1004673321013